Physics of Plasmas

RESEARCH ARTICLE | APRIL 02 2025

Hunting for sources of variability in laser-proton acceleration with thin foils

Ying Gao ; Jianhui Bin ; Daniel Haffa; Jens Hartmann ; Thomas F. Rösch; Florian H. Lindner ; Martin Speicher; Rong Yang ; Tobias M. Ostermayr ; Franz S. Englbrecht ; Peter Hilz; Christian Kreuzer ; Sebastian Lehrack ; Johannes Gebhard; Hao Ding ; Leonard Doyle ; Stefan Karsch; Paul R. Bolton ; Katia Parodi ; Wenjun Ma ; Jörg Schreiber

Phys. Plasmas 32, 043102 (2025)
https://doi.org/10.1063/5.0246173

Physics of Plasmas ARTICLE pubs.aip.org/aip/pop

Hunting for sources of variability in laser-proton acceleration with thin foils

Cite as: Phys. Plasmas **32**, 043102 (2025); doi: 10.1063/5.0246173
Submitted: 5 November 2024 · Accepted: 12 March 2025 ·
Published Online: 2 April 2025

View Online Export Citation CrossMark

Ying Gao,[1,2,a] Jianhui Bin,[1,3,b] Daniel Haffa,[1] Jens Hartmann,[1] Thomas F. Rösch,[1] Florian H. Lindner,[1] Martin Speicher,[1] Rong Yang,[1] Tobias M. Ostermayr,[1] Franz S. Englbrecht,[1] Peter Hilz,[1] Christian Kreuzer,[1] Sebastian Lehrack,[1] Johannes Gebhard,[1] Hao Ding,[4,5] Leonard Doyle,[1] Stefan Karsch,[4,5] Paul R. Bolton,[1] Katia Parodi,[1] Wenjun Ma,[2,c] and Jörg Schreiber[1,d]

AFFILIATIONS

[1]Lehrstuhl für Medizinphysik, Fakultät für Physik, Ludwig-Maximilians-Universität München, 85748 München, Germany
[2]State Key Laboratory of Nuclear Physics and Technology, School of physics, Peking University, Beijing 100871, China
[3]State Key Laboratory of High Field Laser Physics and CAS Center for Excellence in Ultra-Intense Laser Science, Shanghai Institute of Optics and Fine Mechanics, Chinese Academy of Sciences, Shanghai 201800, China
[4]Lehrstuhl für Experimentalphysik - Laserphysik, Fakultät für Physik, Ludwig-Maximilians-Universität München, 85748 München, Germany
[5]Max-Planck-Institut für Quantenoptik, 85748 München, Germany

[a]**Author to whom correspondence should be addressed:** ying_gao@pku.edu.cn
[b]**Electronic mail:** jianhui.bin@siom.ac.cn
[c]**Electronic mail:** wenjun.ma@pku.edu.cn
[d]**Electronic mail:** joerg.schreiber@lmu.de

ABSTRACT

Laser ion acceleration experiments with increasing repetition rates have become more common in recent years. This allows for the study of the stability of proton beam parameters and the search for correlations with laser, target, and positioning system parameters. We conducted a trial experiment with 971 shots and determined key parameters using a variety of optical and proton detectors that are common in many experimental setups. Our findings can be helpful for planning future campaigns and assessing the relevance of certain diagnostics in the effort to monitor performance and improve the stability of future high-repetition-rate systems.

I. INTRODUCTION

The field of laser-driven ion acceleration has witnessed remarkable progress over the past three decades, with maximum energy levels increasing from 1 to 150 MeV.[1–5] This evolution has significantly broadened the scope of applications for laser-driven ion sources, which are characterized by their unique features,[6–9] including picosecond bunch durations, synchronization with laser pulses, small source sizes, and wide energy spectra. These attributes render them particularly suitable for diverse applications, such as radiographic density diagnosis,[10] isochoric heating of matter,[11] and probing transient electric and magnetic fields.[12] As a complementary technology to traditional radio frequency (RF) acceleration sources, laser-driven ion acceleration continues to attract attention for its potential to revolutionize various scientific and industrial fields, including medical therapies,[13] materials science,[14,15] and fundamental physics research.[16]

Despite these advancements, the field faces several challenges that must be addressed to fully realize the potential of laser-driven ion sources. The primary challenge is achieving stable operation, which is critical for many applications that require precise control over the ion bunch parameters. Fluctuations in proton emission can arise from various factors, including variations in laser input parameters, target characteristics, and positioning accuracy. Continuous, noninvasive monitoring of the ion bunch is essential for identifying key experimental parameters and quantifying their impact on proton bunch stability. As the demand for high-repetition-rate systems increases, understanding and mitigating

these fluctuations becomes increasingly important for advancing the technology.

In this context, our work focuses on evaluating proton source stability and sensitivity within a 0.5 Hz laser-proton acceleration system. We have established a comprehensive monitoring framework at our laser-driven proton source, utilizing the ATLAS300 laser system alongside a nano-foil target positioning system (nFTPS) capable of providing a new target every 2 s.[17] Our study employs eight real-time and two offline diagnostics to extract 12 observables for each shot, allowing for an in-depth analysis of proton emission characteristics. Through an analysis of 971 shots, we identify key factors—such as target thickness, laser energy, positioning accuracy, and amplified spontaneous emission (ASE) pedestal length—that contribute to fluctuations in proton parameters. By addressing these challenges, our research aims to enhance the stability and reliability of laser-driven ion sources, thereby paving the way for future advancements in high-repetition-rate systems and their applications. This work is based in part on the doctoral dissertation of one of the authors,[18] and the relevant data processing methods can be referenced for further details. This study identifies the key control variables affecting proton energy stability: target thickness and defocus distance. By keeping these variables within specific ranges, a relatively stable output of proton energy can be achieved, thereby promoting the potential applications of laser-driven protons.

II. RESULTS

The experimental setup and employed instruments are depicted in Fig. 1. A 30 fs laser pulse with a central wavelength of 800 nm was focused onto the target using a 90° off-axis parabolic mirror (OAP). The full-width at half-maximum (FWHM) diameter of the focal spot was 3.3 μm. Considering a laser energy of 4.8 J before the compressor and a transmission efficiency to the target of 49.5%, approximately 30% of the energy was focused within the FWHM of the focal spot. Thus, the peak intensity on target was estimated to be 2.8×10^{20} W/cm^2 based on high-dynamic-range (HDR) focal spot imaging.[19] All laser energy measurements were cross-calibrated using an energy meter to reflect the value before the compressor entrance. The Rayleigh length, which represents the distance over which the beam area doubles, can be determined using the following relationship: $z_R = \frac{\pi FWHM^2}{2ln(2)\lambda}$, where FWHM = 3.3 μm and λ = 800 nm is the laser wavelength. Based on this formula, the Rayleigh length is calculated to be approximately 30.8 μm.

Behind the last telescope in the laser system, a charge-coupled device (CCD) is used to capture a near-field image of the laser pulse. Incident laser energy E1 was obtained by integrating signals from the near-field image. Similarly, the incident energy E2 of the laser could also be obtained by integrating the far-field image, which was recorded by another CCD camera that imaged a scattering screen on which the lens-focused light leaks from the turning mirror before the laser enters the experimental chamber. The center of mass of the far-field image represented the pointing position P for monitoring the shot-to-shot fluctuation of the laser focus position. The correlation of this measure to the on-target focus position was validated prior to experiments at reduced laser power by comparison to the focus image provided by the high-magnification microscope. A spectrometer recorded the spectrum Si of the incident laser pulse from the same scatter screen. The integration of Si in the range 750–850 nm could be used as a third incident energy reference. In addition, the real-time measurement of the incident spectrum could reveal problems of the laser system on a shot-to-shot basis, thereby enabling the identification of "bad shots." The transmission image was detected by a CCD camera that imaged a

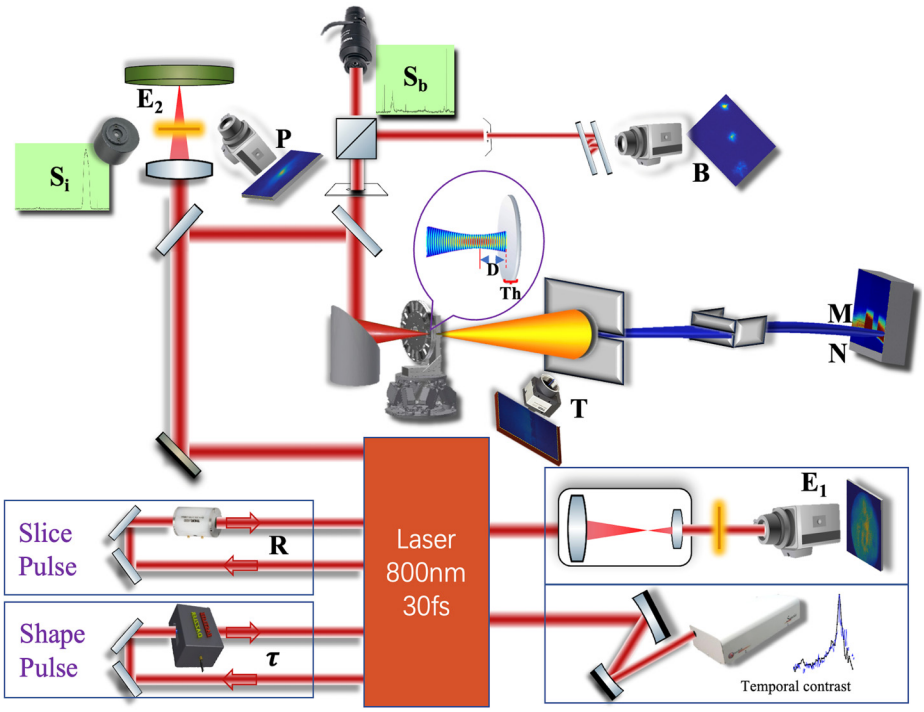

FIG. 1. Schematic of experimental setup. Different uppercase letters indicate different instruments and extracted observables as described below. B is the integral of the charge-coupled device (CCD) counts in the selected non-saturated backscattering image after background subtraction—(backscatter/reflection at mainly 2ω). D is the defocus controlled via nFTPS. E1 is the incident laser energy obtained from the near-field pixel integrated image. E2 is the incident laser energy obtained from the far-field pixel integrated image. M is the maximum kinetic energy and N is the ion number per msr in energy band 2.5–10 MeV, both measured by a wide-angle spectrometer. P is the pointing position from far-field image, R is the trigger time for fast Pockels cell prior to the intensity peak of the laser pulse, Si is the incident laser pulse spectrum ranging from 750 to 850 nm, Sb is the backscatter spectrum integral ($Sb_{2\omega}$: 350–450 nm; Sb_{ω}: 800–1000 nm), T is the transmittance, Th is the target thickness (measured prior to irradiation), and τ is the pulse duration controlled by Dazzler. The temporal intensity curve was measured using a third-order autocorrelator.

screen located ∼50 cm behind the target in the laser-propagation direction. Transmittance (T) is defined as the ratio of the pixel-wise integration of transmitted light intensity to that of the reference empty shot.

The protons emitted from the target were analyzed by a wide-angle spectrometer equipped with RadEye1 CMOS sensors.[20,21] The two-dimensional image allowed for retrieving the energy spectrum (and the angular distribution) of a fraction of the beam, from which the maximum kinetic energy M and the particle number per millisteradian (msr) N at different angles between −2° and 2° at target normal were measured. The backscattered light was collected by the OAP mirror, guided out of the vacuum chamber, and refocused onto a camera. Two nearly parallel silver mirrors were inserted between the lens and camera and served to replicate the backscatter image.[22,23] The replicas of the backscattered light therefore represent laser intensity distributions at different focal planes. Typically, five spots were fit onto the chip and the setup was adjusted to minimize the size of the central replica when a target was in best focus. A displacement of the smallest replica from this original position for a certain laser shot indicates that the target was not in the anticipated longitudinal position, i.e., it could yield the defocusing condition of the laser focus on the target and should be related to the active displacement that we measured via D. We found the quantitative evaluation of this measure rather complicated and restricted the use of this tool to estimate the strength of the backscatter signal. Among the five replicas, at least one was not saturated and could be integrated to yield a (not absolutely calibrated) measure that is proportional to B. The spectrum Sb of this backscattered light was also simultaneously detected in the second arm of this diagnostic. $Sb_{2\omega}$ and Sb_{ω} represent the intensity integral of the second harmonic generation (SHG) spectrum (350–450 nm, 2ω light) and the original spectrum after redshift (800–1000 nm, ω light), respectively.

An acousto-optic programmable dispersion filter (called "DAZZLER"[24]) is used to adjust the pulse duration (τ). In addition, a fast Pockels cell located after the regenerative amplifier is activated at time R (before the main pulse peak) to modify the duration of the ASE (amplified spontaneous emission) pedestal. As described in Ref. 25,

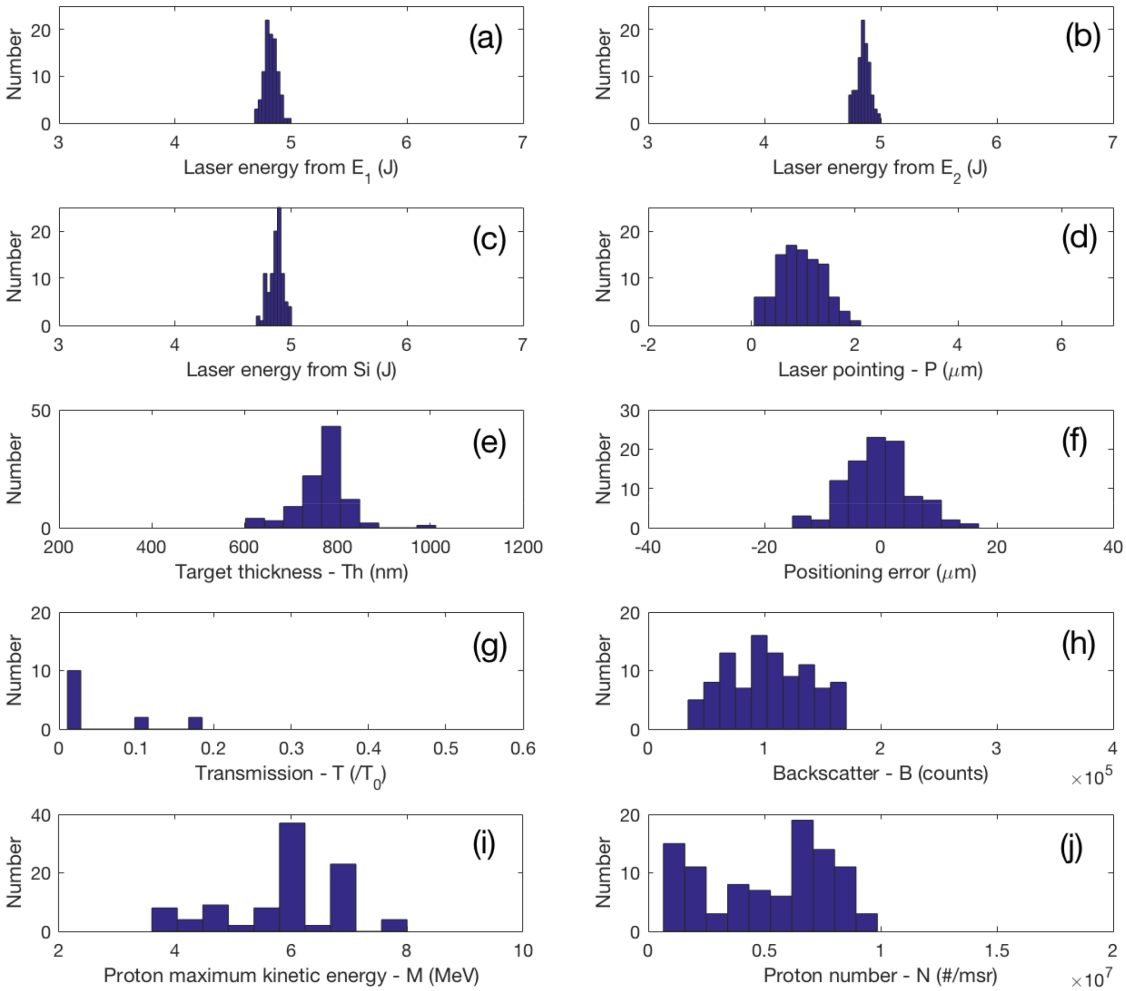

FIG. 2. Histograms of the shot-to-shot variability of non-controllable parameters (a)–(f) and the corresponding monitoring data (g)–(j) for 99 shots. The uppercase letters correspond to the parameters indicated in Fig. 1.

this approach also allows filtering of short prepulses that arrive before the trigger time. Before the experiment, over 1000 plastic foil targets were affixed onto the nFTPS. The self-supporting plastic foil targets were fabricated using Formvar, a polymer dissolved in a suitable solvent. The resulting solution was deposited onto a water surface, where the solvent rapidly evaporated, forming a thin membrane. This membrane was then transferred onto a target holder with a predefined hole pattern. The entire procedure is referred to as the floating method.[26] The initial density of the Formvar material is approximately 1.3 g/cm^3. The thickness of each foil, denoted as Th, was measured using an optical confocal microscope before installation into the target wheel. We conducted a preliminary run to verify the accuracy of our repositioning procedure, achieving a longitudinal precision of $\pm 8\,\mu$m, consistent with prior results.[17] For each shot, we adjusted a specific active displacement parameter, D, in 25 μm increments. We measured the temporal intensity curve using a third-order autocorrelator. The contrasts of the prepulses, occurring at approximately -660 ps and -500 ps relative to the main peak, were slightly below 10^{-6}.[27] Additionally, the ASE pedestal was measured to be around 10^{-9}.

The first dataset includes shots using full laser energy and 99 targets. Figures 2(a)–2(f) illustrate the statistical distributions of laser energy from E_1, E_2 and Si, laser pointing P, target thickness Th, and positioning accuracy. The average incident laser energy E_1 was 4.8 J with a standard deviation of 0.06 J, consistent with E_2 and Si measurements [Figs. 2(a)–2(c)]. Laser pointing was precise, with deviations of only 0–2 μm between the actual laser focus position (P) and the reference position based on attenuated pulse energy [Fig. 2(d)]. The lateral displacement of the focal spot between laser shots, known as jitter, is caused by small vibrations that affect the alignment of optical components, leading to noticeable focus position changes. Consecutive focus images showed a maximum deviation of less than 2 μm, which is comparable to the full width at half-maximum (FWHM) of the focal spot. Given a laser focusing length of 20 cm, this jitter translates to a pointing deviation of less than 10 μrad, which does not cause significant optical aberrations or astigmatism in the experiments. The thickness distribution of the plastic film, shown in Fig. 2(e), was estimated to be 800 nm using the droplet production method,[26] while the measured average thickness was 780 nm with a standard deviation of 60 nm. The nFTPS achieved a longitudinal position accuracy of $\pm 8\,\mu$m within a 95% confidence interval [Fig. 2(f)].

Significant fluctuations in transmittance (T) and backscatter light (B) are shown in Figs. 2(g) and 2(h). Some transmission data are missing due to trigger failures or electromagnetic pulse (EMP) interference. Out of 99 shots, 60 recorded proton maximum kinetic energies, M, between 6 and 7 MeV, while the remaining shots ranged from 3.5 to 8 MeV [Fig. 2(i)]. The proton number per millisteradian (msr) (N) in the 3.5–8 MeV energy band varied by an order of magnitude [Fig. 2(j)]. The initial results confirm that parameters like laser energy and target thickness exhibit normal fluctuations. However, proton bunch parameters, particularly the maximum kinetic energy and, to an even greater extent, the number of protons per steradian, demonstrate significant variability.

We present detailed studies on how various parameters affect outcomes, focusing on target thickness (Fig. 3), target displacement along the laser-propagation direction (Fig. 4), laser pulse duration (Fig. 5), and ASE duration (Fig. 6). Each data point represents a single shot. Results are averaged where appropriate, with mean values and standard deviations shown as error bars. While the instrumentation suite can provide up to twelve observables per shot, we focus on the key metrics, maximum proton energy (M) and number per steradian (N), along with other observables that demonstrate clear trends. This approach aims to identify crucial diagnostics that correlate with proton bunch parameters and could potentially aid in noninvasive proton bunch monitoring, complementing the wide-angle spectrometer.

The impact of target thickness on proton source characteristics, such as maximum kinetic energy (M), proton number per millisteradian (N), and various measurements—including the backscatter image pixel integral of an unsaturated spot (B), backscatter spectra integral (Sb), and transmittance (T)—is illustrated in Fig. 3. The target thickness was varied from 100 to 1000 nm. Results show that both proton number and maximum kinetic energy increase with target thickness. A similar trend is observed in backscattered light measurements (both $Sb_{2\omega}$ and Sb_{ω}). In contrast, transmittance T decreases as target thickness increases. It is noteworthy that the large fluctuation in target thickness itself on the 700 nm target holder leads to large fluctuations in the measured M and N.

The observed dependence of all measurements on target thickness consistently points to a laser contrast-related issue. Thinner targets experience significant damage before the main intensity peak arrives, leading to a deterioration in the acceleration conditions. This

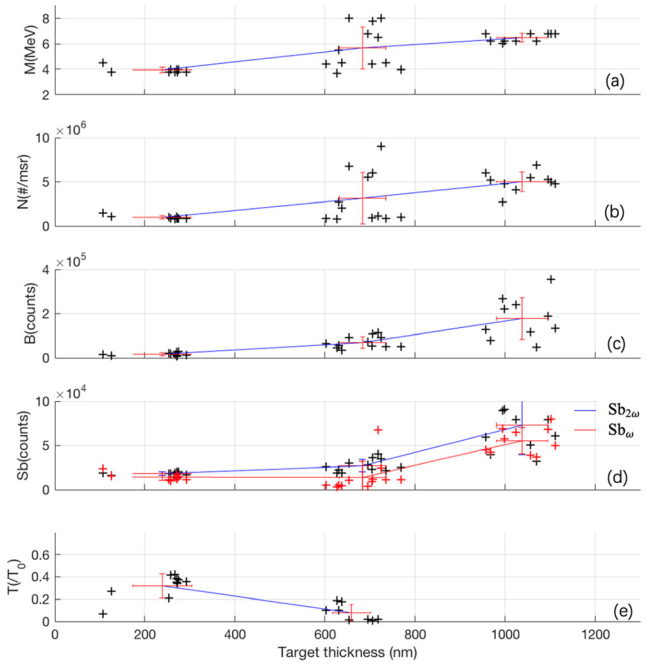

FIG. 3. Influence of thickness variation on proton and other quantities. The plot includes M—maximum kinetic energy (a) and N—the proton number per millisteradian (b), as measured by the wide-angle spectrometer; B—pixel integral of an unsaturated spot in the backscatter image (c); Sb—pixel integral of backscatter spectra ($Sb_{2\omega}$: 350–450 nm; Sb_{ω}: 800–1000 nm) (d); and T—the transmittance (e). Note that some transmission data are missing due to trigger issues or electromagnetic pulse (EMP) interference.

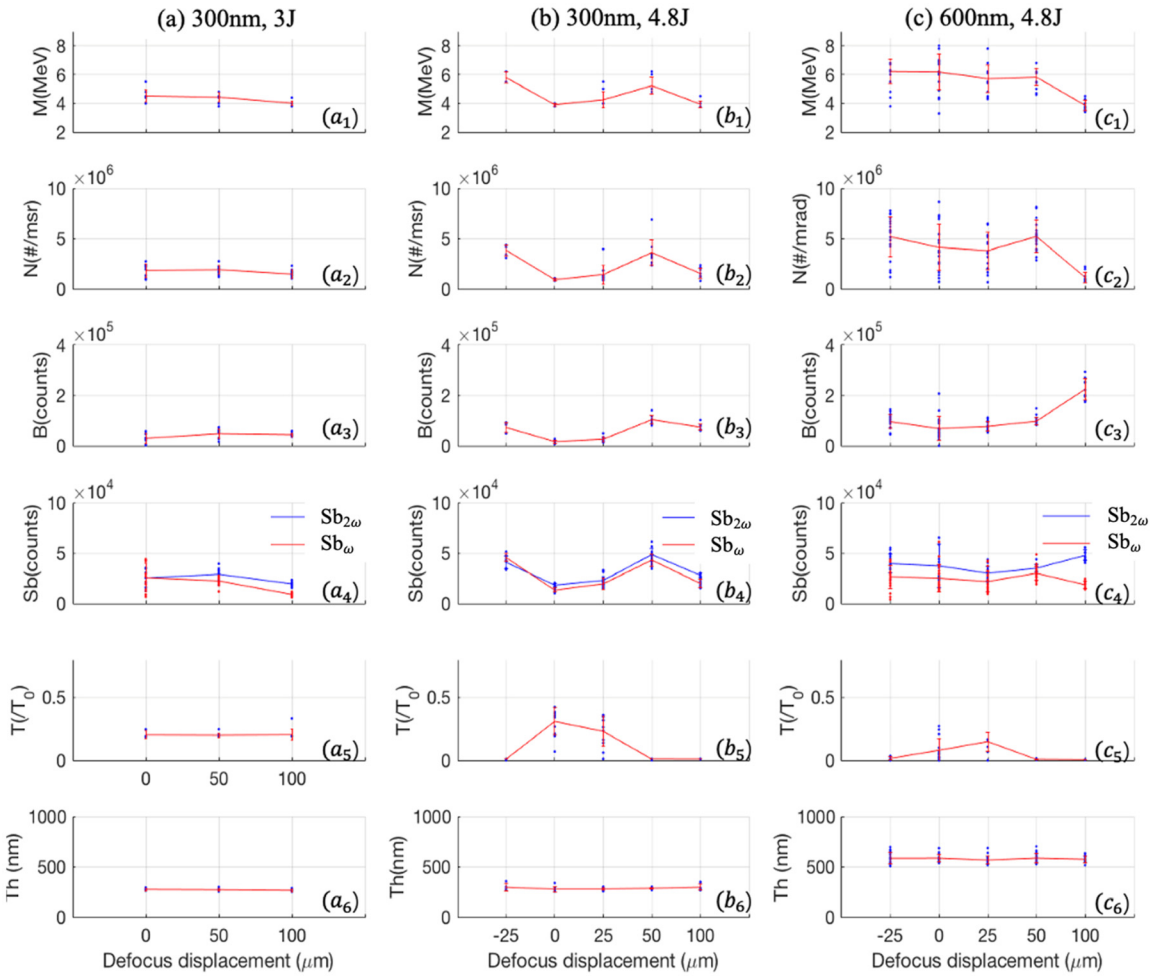

FIG. 4. Influence of defocus displacement variation on proton and other quantities in three cases: (a) Th = 300 nm and $E_1 = 3$J; (b) Th = 300 nm and $E_1 = 4.8$J; (c) Th = 600 nm and $E_1 = 4.8$J. The symbols +/- indicate the target position relative to the laser focal plane (upstream/downstream). The capital letters M, N, B, Sb, T, and Th in subplots (a_1)–(a_6), (b_1)–(b_6), and (c_1)–(c_6) retain the same definitions as those in Fig. 1. Target thickness is plotted against defocus displacement to exclude its effects.

early onset of target expansion results in increased transmission and reduced reflection in thinner targets compared to thicker ones. These effects highlight the critical role of laser contrast in high-intensity laser–target interactions, particularly for thin foil targets. This conclusion can be further validated in the following experiments by employing Pockels cell filtering of prepulses (Fig. 6). Specifically, proton acceleration is more effective when triggered closer to the main pulse. In addition, the acceleration process can be optimized by examining the relationship between proton energy and laser absorption.[23]

The impact of defocus displacement D on the proton source is presented in Fig. 4 across three scenarios: (a) Th = 300 nm and $E_1 = 3$ J (30 shots), (b) Th = 300 nm and $E_1 = 4.8$ J (40 shots), (c) Th = 600 nm and $E_1 = 4.8$ J (90 shots). In case (a), the maximum proton kinetic energy (M), proton number (N), and backscatter spectra integral (Sb) show a slight decrease as D increases from 0 to 100 μm. In case (b), the data for M, N, B, Sb, and T exhibit nearly symmetrical changes around the focal plane, ranging from −25 to 25 μm. At D = 0 μm, the T is highest, while the maximum energy (M) and particle number (N) are at their lowest. Within the range of 0–100 μm, the proton energy (M) and proton number (N) reached their maximum values at a focal position of +50 μm. Similarly, high proton energies and numbers were observed at a focal position of −25 μm. However, considering the potential for increased back-reflection at this defocused position, which could pose a risk to the laser system, we did not further investigate in this direction. In case (c), M and N are not significantly affected by D in the range −25 to 50 μm. At D = 100 μm, M and N are drastically reduced, and the corresponding Sb_ω is also reduced, while $Sb_{2\omega}$ is increased. It indicates that the efficiency of converting ω light into 2ω light increases, but the efficiency for accelerating ions decreases. Combining Figs. 4(a)–4(c), it can be concluded that the effect of defocus distance on the ion bunch is not static but is also related to the choice of target thickness and laser energy, which has been anticipated and observed since the early stages of laser-driven proton acceleration.[25] When the target thickness and laser energy are altered, the optimal defocus distance dynamically changes as well.

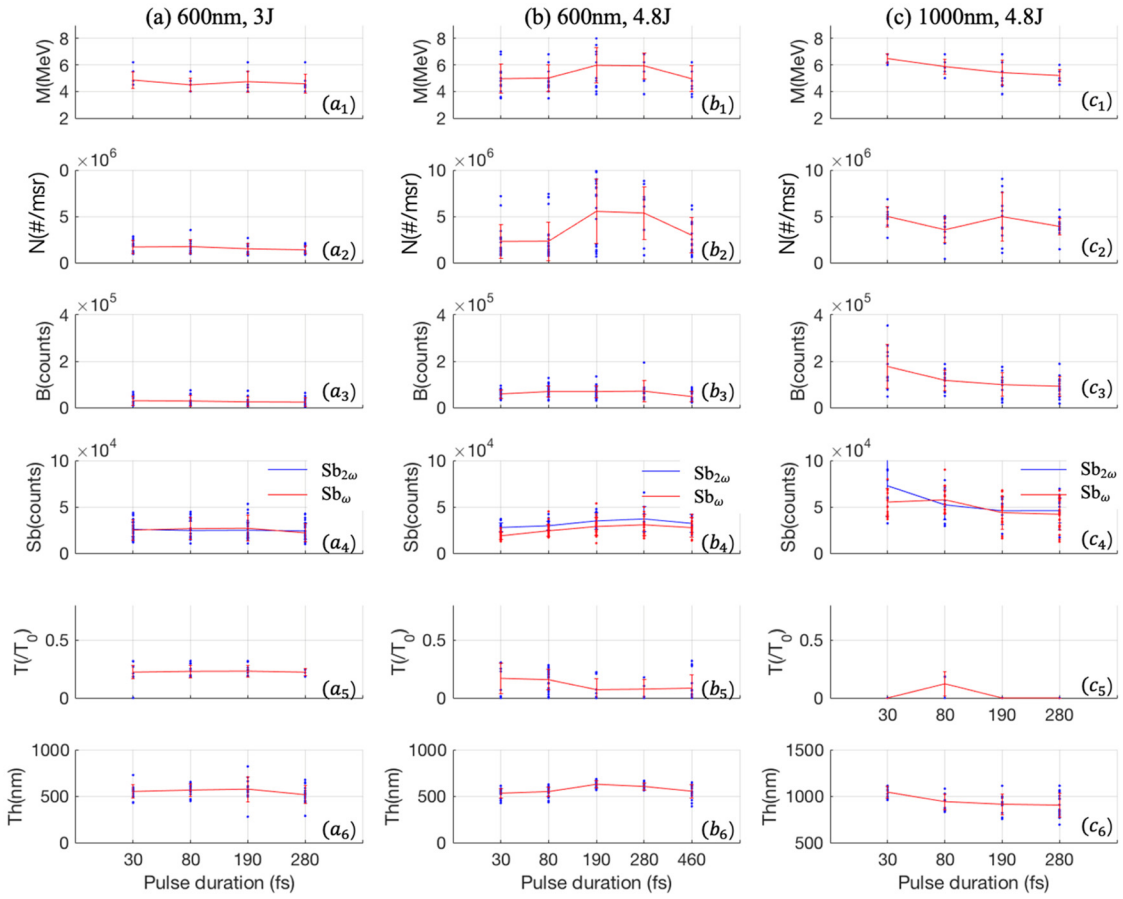

FIG. 5. Influence of laser pulse duration on proton and other quantities in three cases. (a) Target thickness Th = 600 nm and laser energy $E_1 = 3$ J. (b) Th = 600 nm and $E_1 = 4.8$ J. (c) Th = 1000 nm and $E_1 = 4.8$ J. The capital letters M, N, B, Sb, T, and Th in subplots (a_1)–(a_6), (b_1)–(b_6), and (c_1)–(c_6) retain the same definitions as those in Fig. 1. In order to avoid misinterpretation of apparent correlations, the target thickness as a function of pulse duration was intentionally plotted here.

The results for different pulse duration values ($\tau = 30$, 80, 190, 280, and 460 fs) are represented in Fig. 5. Again, three cases are presented: (a) Th = 600 nm and $E_1 = 3$ J, (b) Th = 600 nm and $E_1 = 4.8$ J, (c) Th = 1000 nm and $E_1 = 4.8$ J. The last row shows the target thickness, which, as explained above, could not be kept perfectly constant on a same target holder. In case (a), the pulse duration τ has no significant effect on the proton beam. Case (b) superficially shows a possible dependence on τ, but since similar trends are also observed for maximum energy and number of particles at target thickness, the overall dependence on pulse duration appears to be weak. Furthermore, backscattered light, spectral integration, and transmission are largely unaffected. A similar pattern is observed in case (c). In all three cases (a-c), the proton yield does not have a strong dependence on the laser pulse duration.

The effect of the duration of the ASE plateau or prepulses on the proton bunch is illustrated in Fig. 6. A trigger time of −700 ps indicates that the fast Pockels cell is activated 700 ps before the main laser peak. Reducing the trigger time can shorten the ASE plateau and eliminate the preceding prepulses, which leads to the observed increase in proton energy and number. The default trigger time was set at −500 ps for all other measurements. In addition to using fast Pockels cells, another effective method for removing prepulses is the utilization of plasma mirrors. Plasma mirrors reduce ASE noise and prepulses by reflecting the main pulse while allowing lower-intensity ASE to dissipate, as a result, enhancing the temporal contrast.[28]

To enhance the practical applications of laser-driven proton beams, we explored their stability and dependence on various experimental parameters. By analyzing a substantial amount of experimental data, we focused on varying one parameter at a time while keeping others constant to achieve a more stable proton beam with adjustable energy. As shown in Fig. 7, increasing the target's average thickness from 300 nm to 600 nm (with a thickness error of ±100 nm) significantly increases both the number of protons and their energy, with the average maximum energy rising from 4.8 to 7.2 MeV. However, when the thickness is increased to 900 nm, although some maximum energies exceed 10 MeV, the average energy does not significantly increase, and stability worsens. This instability is likely due to two main factors: first, the non-uniformity of the target thickness, which can be exacerbated by the droplet method; second, the interaction of different acceleration mechanisms within that thickness range, such as plasma

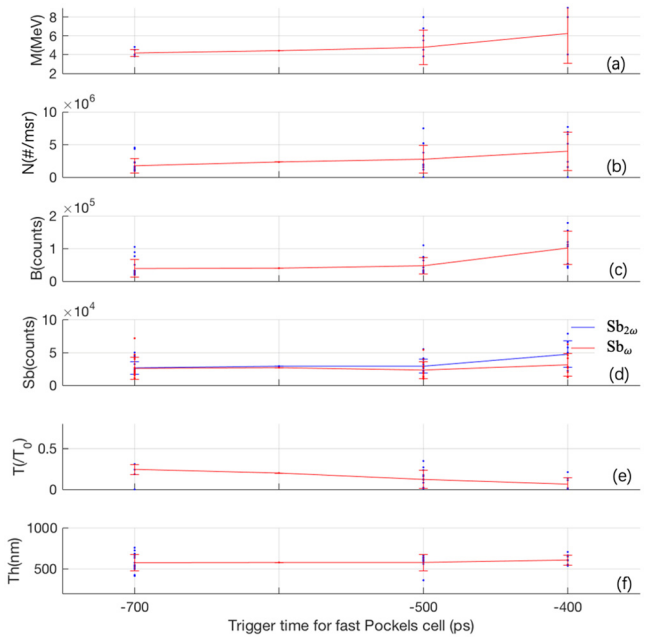

FIG. 6. Effect of trigger time on protons and other quantities. To eliminate the effect of target thickness, we present the target thickness (Th) plotted against trigger time. The capital letters M, N, B, Sb, T, and Th in subplots (a)–(f) retain the same definitions as those in Figs. 1(a)–1(f).

expansion and radiation pressure acceleration, which can lead to complex and less stable acceleration dynamics.[23] Further research is needed to understand better and optimize these interactions. To improve stability, we recommend using a spin-coating method for better control over the thickness.

Assuming we can maintain the target thickness error within 10% (e.g., 600 nm ± 50 nm), we can select the relevant shots for statistical analysis. As illustrated in Fig. 8, adjusting the defocus from 0 μm to ±25 μm, +50 μm, and then to +100 μm results in a significant reduction in the average maximum proton energy—from nearly 9 MeV down to 6 MeV, and further to 4 MeV. This demonstrates that controlling the defocus distance effectively stabilizes proton energy output, providing a reliable method for adjusting proton beam energy while maintaining beam stability. Furthermore, adjusting the defocus appears to be a more reliable method for tuning proton energy by altering the laser intensity. However, this approach assumes that the target thickness is uniformly controlled within ±10%. It is anticipated that if the thickness uniformity can be improved further, proton beam stability will be significantly enhanced.

The maximum energy (M) and particle number (N) show similar patterns across various parameters, as shown in Fig. 9. The blue asterisks represent the data obtained from our experimental work. The data of other shapes and colors are transformed from the published experimental data of multiple international laboratories. This figure summarizes the relationship between the proton number and the cutoff energy in an exponential coordinate form. It is worth noting that these experimental data do not distinguish between laser parameters, target parameters, or even acceleration mechanisms. The purpose of this treatment is to investigate whether the positive correlation between the proton number and the cutoff energy is independent of the above-mentioned factors. When we conduct statistics on all the data, the laser energy on target ranges from 0.7 J[37] to 210 J,[4] the pulse width is from 30 fs[5] to 0.9 ps,[4] the target thickness ranges from 5.3 nm,[37] 58 nm[30] to 10 μm,[34] and the target materials include plastic foil,[4,5,31–33,35] plastic sphere,[36] Al,[33] Au[34] and even hydrogen jet.[29] From the perspective of acceleration mechanisms, the data encompass proton beams based on various mechanisms, such as target normal sheath acceleration (TNSA),[31] radiation pressure acceleration (RPA),[37] break-out

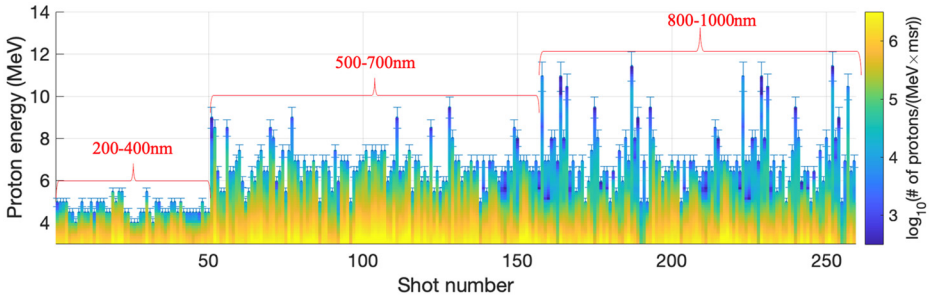

FIG. 7. Proton energy spectra of 258 shots, categorized by target thickness. $\tau = 30$ fs, E1 = 4.8 J, D = 0 μm, trigger time at −500 ps.

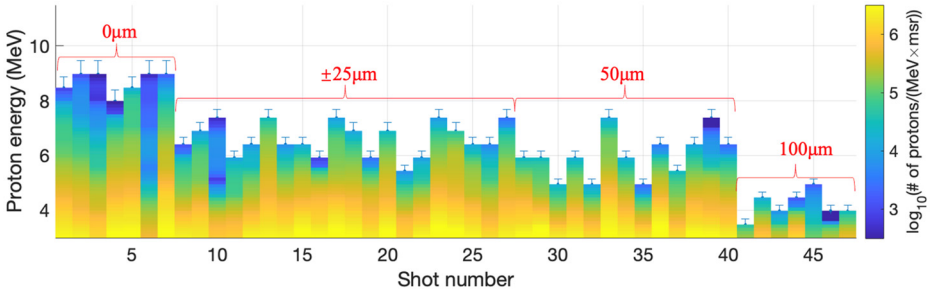

FIG. 8. Proton energy spectra of 47 shots, categorized by defocus D. $\tau = 30$ fs, E1 = 4.8 J, Th = 600 nm (±50 nm), trigger time at −500 ps.

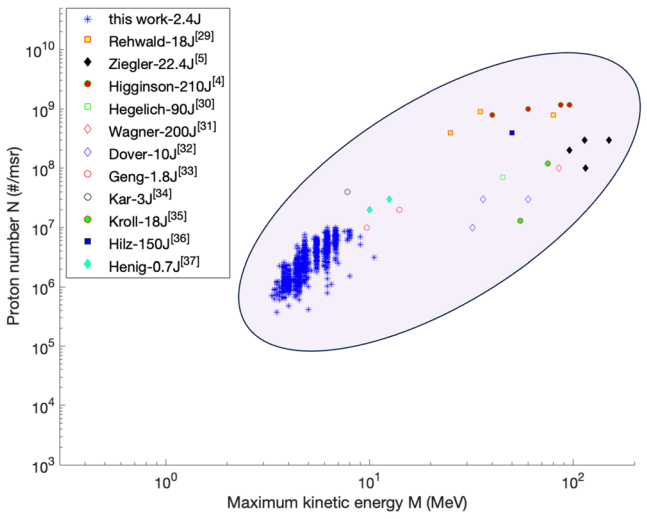

FIG. 9. Proton number per msr N as a function of maximum kinetic energy M in the case where no parameters, such as laser, target, and positioning, are distinguished. In addition to the blue asterisk data (this work), the other data are derived from previously published literature and are estimated through unit conversion. The laser energy on target and corresponding references are shown in the legend.

afterburner (BOA),[30] relativistically induced transparency (RIT),[5] Coulomb explosion,[36] and hybrid RPA-TNSA.[4]

Based on the statistical analysis, we observe that the positive correlation between proton number and cutoff energy is to some extent independent of laser and target parameters, and appears to be unaffected by the specific acceleration mechanism. This can be attributed to the fact that the proton energy spectrum typically displays an exponential decay, even though certain acceleration mechanisms may produce quasi-monoenergetic peak features.[5,36,37] Achieving a higher proton cutoff energy generally requires a larger proton population, which, in turn, necessitates greater laser energy absorption efficiency. The extensive range of experimental parameters underscores the robustness of the observed correlation between proton number and cutoff energy, suggesting that this relationship is a fundamental characteristic that transcends specific experimental conditions. By considering the region where the data points of this work fall in Fig. 9, along with the information provided in Figs. 3 and 6, we have reason to believe that we did not conduct experiments within the optimal target thickness range. Under our current laser temporal contrast conditions, the optimal target thickness is greater than 1 micrometer. When the thickness is below this value, the stability of the proton beam output is significantly compromised.

From Fig. 9, we also observe that higher laser energy generally holds the potential for generating both higher proton energies and larger proton populations, although this is not an absolute rule. The efficacy of this process is influenced by the coupling between the laser and the target, particularly the laser energy absorption efficiency, which is a crucial factor to consider. This is the next key aspect we will discuss in detail.

III. DISCUSSION

The observed proton energy spectra characteristics, combined with laser and target parameters, suggest that the proton acceleration predominantly follows the target normal sheath acceleration (TNSA) mechanism. For a laser normalized intensity of $a_0 \cong 8.5 \times 10^{-10}\left[\lambda(\mu\mathrm{m})\right]\sqrt{I_0(\mathrm{W/cm^2})} \approx 11.9$ and a target thickness $d = 1\,\mu$m, which yields higher proton cutoff energy, the maximum proton energy ϵ_{max} can be estimated using the TNSA scaling law and isothermal expansion model,[38,39]

$$\epsilon_{max} = 2T_{hot}\left[\ln\left(\sqrt{1+t_p^2}+t_p\right)\right]^2,$$

where $T_{hot} = m_e c^2\left(\sqrt{1+a_0^2}-1\right)$ denotes the hot electron temperature. The normalized acceleration time $t_p = \frac{\omega_p t_{acc}}{\sqrt{2}\exp 1}$ depends on the proton acceleration time $t_{acc} \propto (\tau_{laser} + \tau_{min})$.[40,41] For ultrashort laser pulses, τ_{min} (the proton–electron energy transfer time) ranges between 60 and 100 fs,[40–42] and 60 fs is adopted here. The ion plasma frequency $\omega_p = \sqrt{\frac{Z_i n_{e0} e^2}{m_i \varepsilon_0}}$ incorporates the hot electron density $n_{e0} = \frac{N_e}{c\tau_{laser} S_{sheath}}$, where $N_e = \frac{fE_L}{T_{hot}}$ (number of electrons), $f \approx 20\%$ (laser-to-electron conversion efficiency),[43] and $S_{sheath} = \pi(r_0 + d\cdot\tan\theta)^2$ (sheath field area). With $E_L = 0.72$ J (30% of 2.4 J), $r_0 = 3.3\,\mu$m, $\tau_{laser} = 30$ fs, and $\theta \approx 10°$,[43] the calculated $\epsilon_{max} \sim 24.7MeV$ exceeds the experimentally measured maximum cutoff energy of 11.5 MeV for 1 μm targets. This discrepancy arises from the 1D model's neglect of transverse sheath field distribution and three-dimensional electron transport effects.[44]

Notably, the experimental observation of decreasing proton energy with reduced target thickness (Fig. 3) contradicts standard TNSA predictions, indicating significant prepulse influence. Preplasma formation induced by prepulses alters the effective target thickness through premature ionization, thereby reducing sheath field density gradients and consequently deteriorating acceleration performance. This is the basis for the existence of an optimal target thickness under specific laser conditions, where the pre-plasma screening and the interaction intensity of the target and the main pulse reach a dynamic equilibrium.[22] Defocusing laser mitigates prepulse effects, explaining the enhanced proton energy at small defocusing distances. However, excessive defocusing (e.g., 100 μm) degrades both proton energy and yield [Fig. 4(b)] due to reduced peak laser intensity.

While employing a Pockels cell suppresses prepulse effects and improves proton energy, timing jitter introduces fluctuations in energy and yield [Figs. 6(a) and 6(b)], highlighting operational sensitivity to prepulse dynamics. To stabilize proton sources, experimental parameters should operate in prepulse-insensitive regimes, complemented by plasma mirrors for prepulse suppression. Concurrently, precise target positioning and thickness control are critical for ensuring stable proton beam output.

Analysis of the data shows an inverse relationship between transmission (T) and backscatter (B). Figure 10 illustrates this correlation, plotting transmittance values against the corresponding backscatter signals. The color coding of the points indicates the maximum kinetic energy (M) in panel (a) and the proton number per msr (N) in panel (b). A strong negative correlation exists between high proton yield and low transmittance. Although the data exhibit considerable variability, the diagnostics of backscattered and transmitted light demonstrate significant potential as complementary performance monitors for laser-driven ion sources.

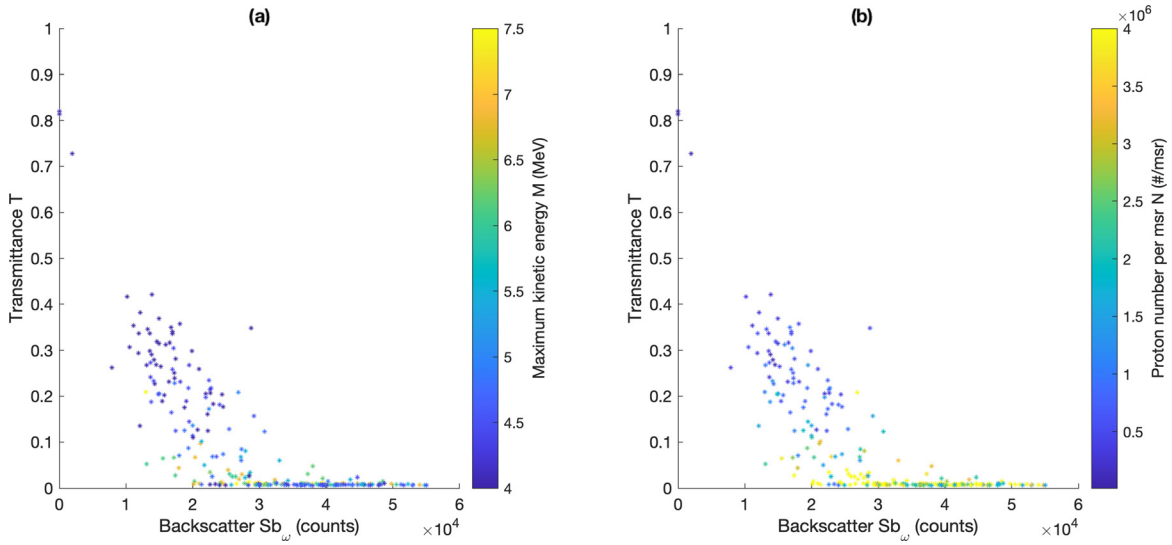

FIG. 10. Transmittance T as a function of backscatter signal Sb_ω in the case where no parameters such as laser and target are distinguished. The color denotes the maximum kinetic energy M and the proton number per msr N in (a) and (b), respectively.

Estimating energy absorption is essential, as the efficiency of converting laser energy to particle energy relies heavily on the amount of absorbed energy. While our backscatter energy monitor lacks absolute calibration, we define laser light absorption as $\eta = 1 - R - T$, where R is reflectance and T is measured transmittance. It is important to note that backreflection refers to backscattered light post-redshift, assumed to have a linear relationship. We normalize the backscatter signals $Sb_\omega = 10 \times 10^4$ and $Sb_\omega = 6 \times 10^4$ to 1, ensuring η ranges from 0 to 1, as illustrated in Figs. 9(a) and 9(b). Regardless of the normalization method, the maximum absorptivity η consistently appears in the red circle region. Additionally, when comparing the blue circled area of Fig. 11 with the corresponding area in Fig. 10, we find that the highest η does not necessarily correspond to the largest proton number.

IV. CONCLUSION

In conclusion, we have developed a laser-driven proton accelerator capable of operating at 0.5 Hz and adjustable energy levels. Effective monitoring of laser-driven ion sources, combined with complementary diagnostics, is essential for optimizing performance and stability. While our current instrumentation reveals fluctuations potentially linked to the limited temporal contrast of laser pulses, improving this aspect is critical. Additionally, precise control of target thickness can enhance the stability of ion energy, allowing for effective modulation through defocusing. Characterizing both transmitted and backscattered light can help identify key parameters, influencing ion source performance, leading to refined experimental setups and improved reliability. This

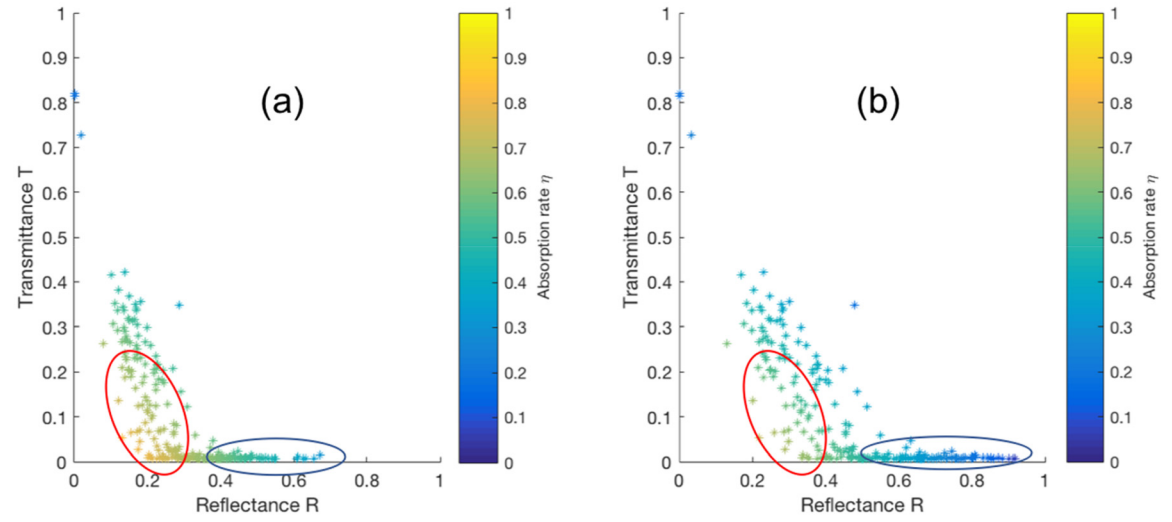

FIG. 11. Absorption rate η derived by transmittance T and reflectance R. R is the respective normalized Sb_ω by $Sb_\omega = 10 \times 10^4$ (a) and $Sb_\omega = 6 \times 10^4$ (b).

comprehensive approach is vital for advancing laser-driven ion acceleration technology and its diverse applications.

ACKNOWLEDGMENTS

We acknowledge the support of the DFG-funded cluster of excellence Munich-Centre for Advanced Photonics, the support of the National Grand Instrument Project (SQ2019YFF010006), the National Natural Science Foundation of China (11775010 and 61631001), and NSFC innovation group project (11921006). J.B. is funded by a Feodor Lynen Fellowship of the Alexander von Humboldt Foundation. T.F.R. acknowledges support from the German Academic Scholarship Foundation. F.H.L. acknowledges funding by BMBF under Contract No. 05P15WMEN9.

AUTHOR DECLARATIONS

Conflict of Interest

The authors have no conflicts to disclose.

Author Contributions

Ying Gao: Conceptualization (equal); Data curation (equal); Formal analysis (equal); Investigation (equal); Methodology (equal); Writing – original draft (equal); Writing – review & editing (equal). **Jianhui Bin:** Conceptualization (lead); Investigation (lead); Methodology (lead); Writing – original draft (lead); Writing – review & editing (lead). **Daniel Haffa:** Investigation (equal); Methodology (equal); Validation (equal). **Jens Hartmann:** Investigation (equal); Methodology (equal); Validation (equal). **Thomas F. Rösch:** Investigation (equal); Methodology (equal); Validation (equal). **Florian H. Lindner:** Investigation (equal); Methodology (equal); Validation (equal). **Martin Speicher:** Investigation (equal); Methodology (equal); Validation (equal). **Rong Yang:** Investigation (equal); Methodology (equal); Validation (equal). **Tobias M. Ostermayr:** Investigation (equal); Methodology (equal); Validation (equal). **Franz S. Englbrecht:** Investigation (equal); Methodology (equal); Validation (equal). **Peter Hilz:** Investigation (equal); Methodology (equal); Validation (equal). **Christian Kreuzer:** Investigation (equal); Methodology (equal); Validation (equal). **Sebastian Lehrack:** Investigation (equal); Methodology (equal); Validation (equal). **Johannes Gebhard:** Investigation (equal); Methodology (equal); Validation (equal). **Hao Ding:** Investigation (equal); Methodology (equal); Validation (equal). **Leonard Doyle:** Investigation (equal); Methodology (equal); Validation (equal). **Stefan Karsch:** Investigation (equal); Methodology (equal); Validation (equal). **Paul R. Bolton:** Investigation (equal); Methodology (equal); Validation (equal). **Katia Parodi:** Investigation (equal); Methodology (equal); Validation (equal). **Wenjun Ma:** Conceptualization (lead); Investigation (lead); Supervision (lead); Writing – review & editing (lead). **Jörg Schreiber:** Conceptualization (lead); Data curation (lead); Investigation (lead); Methodology (lead); Project administration (lead); Supervision (lead); Writing – original draft (lead); Writing – review & editing (lead).

DATA AVAILABILITY

The data that support the findings of this study are available from the corresponding author upon reasonable request.

REFERENCES

[1]A. P. Fews, P. A. Norreys, F. N. Beg, A. R. Bell, A. E. Dangor, C. N. Danson, P. Lee, and S. J. Rose, "Plasma ion emission from high intensity picosecond laser pulse interactions with solid targets," Phys. Rev. Lett. **73**, 1801 (1994).
[2]R. A. Snavely, M. H. Key, S. P. Hatchett, T. E. Cowan, M. Roth, T. W. Phillips, M. A. Stoyer, E. A. Henry, T. C. Sangster, M. S. Singh, S. C. Wilks, A. MacKinnon, A. Offenberger, D. M. Pennington, K. Yasuike, A. B. Langdon, B. F. Lasinski, J. Johnson, M. D. Perry, and E. M. Campbell, "Intense high-energy proton beams from petawatt-laser irradiation of solids," Phys. Rev. Lett. **85**, 2945 (2000).
[3]Y. Shou, X. Wu, K. H. Pae, G.-E. Ahn, S. Y. Kim, S. H. Kim, J. W. Yoon, J. H. Sung, S. K. Lee, Z. Gong, X. Yan, I. W. Choi, and C. H. Nam, "Laser-driven proton acceleration beyond 100 MeV by radiation pressure and Coulomb repulsion in a conduction-restricted plasma," Nat. Commun. **16**, 1487 (2025).
[4]A. Higginson, R. J. Gray, M. King, R. J. Dance, S. D. R. Williamson, N. M. H. Butler, R. Wilson, R. Capdessus, C. Armstrong, J. S. Green, S. J. Hawkes, P. Martin, W. Q. Wei, S. R. Mirfayzi, X. H. Yuan, S. Kar, M. Borghesi, R. J. Clarke, D. Neely, and P. McKenna, "Near-100 MeV protons via a laser-driven transparency-enhanced hybrid acceleration scheme," Nat. Commun. **9**, 724 (2018).
[5]T. Ziegler, I. Göthel, S. Assenbaum, C. Bernert, F.-E. Brack, T. E. Cowan, N. P. Dover, L. Gaus, T. Kluge, S. Kraft, F. Kroll, J. Metzkes-Ng, M. Nishiuchi, I. Prencipe, T. Püschel, M. Rehwald, M. Reimold, H.-P. Schlenvoigt, M. E. P. Umlandt, M. Vescovi, U. Schramm, and K. Zeil, "Laser-driven high-energy proton beams from cascaded acceleration regimes," Nat. Phys. **20**, 1211 (2024).
[6]H. Daido, M. Nishiuchi, and A. S. Pirozhkov, "Review of laser-driven ion sources and their applications," Rep. Prog. Phys. **75**(5), 056401 (2012).
[7]A. Macchi, M. Borghesi, and M. Passoni, "Ion acceleration by superintense laser-plasma interaction," Rev. Mod. Phys. **85**, 751 (2013).
[8]J. Schreiber, P. R. Bolton, and K. Parodi, "'Hands-on' laser-driven ion acceleration: A primer for laser-driven source development and potential applications," Rev. Sci. Instrum. **87**, 071101 (2016).
[9]P. McKenna, K. W. D. Ledingham, S. Shimizu, J. M. Yang, L. Robson, T. McCanny, J. Galy, J. Magill, R. J. Clarke, D. Neely, P. A. Norreys, R. P. Singhal, K. Krushelnick, and M. S. Wei, "Broad energy spectrum of laser-accelerated protons for spallation-related physics," Phys. Rev. Lett. **94**, 084801 (2005).
[10]A. J. Mackinnon, P. K. Patel, M. Borghesi, R. C. Clarke, R. R. Freeman, H. Habara, S. P. Hatchett, D. Hey, D. G. Hicks, S. Kar, M. H. Key, J. A. King, K. Lancaster, D. Neely, A. Nikkro, P. A. Norreys, M. M. Notley, T. W. Phillips, L. Romagnani, R. A. Snavely, R. B. Stephens, and R. P. J. Town, "Proton radiography of a laser-driven implosion," Phys. Rev. Lett. **97**, 045001 (2006).
[11]P. K. Patel, A. J. Mackinnon, M. H. Key, T. E. Cowan, M. E. Foord, M. Allen, D. F. Price, H. Ruhl, P. T. Springer, and R. Stephens, "Isochoric heating of solid-density matter with an ultrafast proton beam," Phys. Rev. Lett. **91**, 125004 (2003).
[12]B. Dromey, M. Coughlan, L. Senje, M. Taylor, S. Kuschel, B. Villagomez-Bernabe, R. Stefanuik, G. Nersisyan, L. Stella, J. Kohanoff, M. Borghesi, F. Currell, D. Riley, D. Jung, C.-G. Wahlström, C. L. S. Lewis, and M. Zepf, "Picosecond metrology of laser-driven proton bursts," Nat. Commun. **7**, 10642 (2016).
[13]U. Linz and J. Alonso, "What will it take for laser driven proton accelerators to be applied to tumor therapy?," Phys. Rev. Spec. Top. -Accel. Beams **10**, 094801 (2007).
[14]A. Mančić, A. Lévy, M. Harmand, M. Nakatsutsumi, P. Antici, P. Audebert, P. Combis, S. Fourmaux, S. Mazevet, O. Peyrusse, V. Recoules, P. Renaudin, J. Robiche, F. Dorchies, and J. Fuchs, "Picosecond short-range disordering in isochorically heated aluminum at solid density," Phys. Rev. Lett. **104**, 035002 (2010).
[15]A. Pelka, G. Gregori, D. O. Gericke, J. Vorberger, S. H. Glenzer, M. M. Günther, K. Harres, R. Heathcote, A. L. Kritcher, N. L. Kugland, B. Li, M. Makita, J. Mithen, D. Neely, C. Niemann, A. Otten, D. Riley, G. Schaumann, M. Schollmeier, A. Tauschwitz, and M. Roth, "Ultrafast melting of carbon induced by intense proton beams," Phys. Rev. Lett. **105**, 265701 (2010).
[16]D. Habs, P. G. Thirolf, M. Gross, K. Allinger, J. Bin, A. Henig, D. Kiefer, W. Ma, and J. Schreiber, "Introducing the fission–fusion reaction process: Using a

laser-accelerated Th beam to produce neutron-rich nuclei towards the N=126 waiting point of the r-process," Appl. Phys. B **103**, 471–484 (2011).
[17]Y. Gao, J. Bin, D. Haffa, C. Kreuzer, J. Hartmann, M. Speicher, F. H. Lindner, T. M. Ostermayr, P. Hilz, T. F. Rösch, S. Lehrack, F. Englbrecht, S. Seuferling, M. Gilljohann, H. Ding, W. Ma, K. Parodi, and J. Schreiber, "An automated, 0.5 Hz nano-foil target positioning system for intense laser plasma experiments," High Power Laser Sci. Eng. **5**, e12 (2017).
[18]Y. Gao, "High repetition rate laser driven proton source and a new method of enhancing acceleration," Dissertation (Fakultät für Physik, 2020).
[19]J. Hartmann, D. Haffa, M. Speicher, J. Bin, P. Hilz, C. Kreuzer, T. Ostermayr, S. Lehrack, and J. Schreiber, "The spatial contrast challenge for intense laser-plasma experiments," J. Phys: Conf. Ser. **1079**, 012003 (2018).
[20]F. H. Lindner, J. H. Bin, F. Englbrecht, D. Haffa, P. R. Bolton, Y. Gao, J. Hartmann, P. Hilz, C. Kreuzer, T. M. Ostermayr, T. F. Rösch, M. Speicher, K. Parodi, P. G. Thirolf, and J. Schreiber, "A novel approach to electron data background treatment in an online wide-angle spectrometer for laser-accelerated ion and electron bunches," Rev. Sci. Instrum. **89**, 013301 (2018).
[21]S. Reinhardt, W. Draxinger, J. Schreiber, and W. Assmann, "A pixel detector system for laser-accelerated ion detection," J. Instrum. **8**(03), P03008 (2013).
[22]T. F. Rösch, Z. Szabó, D. Haffa, J. Bin, S. Brunner, F. S. Englbrecht, A. A. Friedl, Y. Gao, J. Hartmann, P. Hilz, C. Kreuzer, F. H. Lindner, T. M. Ostermayr, R. Polanek, M. Speicher, E. R. Szabó, D. Taray, T. Tőkés, M. Würl, K. Parodi, K. Hideghéty, and J. Schreiber, "A feasibility study of zebrafish embryo irradiation with laser accelerated protons," Rev. Sci. Instrum. **91**(6), 063303 (2020).
[23]J. H. Bin, K. Allinger, K. Khrennikov, S. Karsch, P. R. Bolton, and J. Schreiber, "Dynamics of laser-driven proton acceleration exhibited by measured laser absorptivity and reflectivity," Sci. Rep. **7**, 43548 (2017).
[24]F. Verluise, V. Laude, Z. Cheng, C. Spielmann, and P. Tournois, "Amplitude and phase control of ultrashort pulses by use of an acousto-optic programmable dispersive filter: Pulse compression and shaping," Opt. Lett. **25**, 575 (2000).
[25]M. Kaluza, J. Schreiber, M. I. K. Santala, G. D. Tsakiris, K. Eidmann, J. Meyer-ter-Vehn, and K. J. Witte, "Influence of the laser prepulse on proton acceleration in thin foil experiments," Phys. Rev. Lett. **93**, 045003 (2004).
[26]S. Seuferling, M. A. O. Haug, P. Hilz, D. Haffa, C. Kreuzer, and J. Schreiber, "Efficient offline production of freestanding thin plastic foils for laser-driven ion sources," High Power Laser Sci. Eng. **5**, e8 (2017).
[27]M. Speicher, D. Haffa, M. A. O. Haug, J. Bin, Y. Gao, J. Hartmann, P. Hilz, C. Kreuzer, F. H. Lindner, T. M. Ostermayr, T. F. Rösch, R. Yang, and J. Schreiber, "Integrated double-plasma-mirror targets for contrast enhancement in laser ion acceleration," J. Phys: Conf. Ser. **1079**, 012002 (2018).
[28]S. Inoue, K. Maeda, S. Tokita, K. Mori, K. Teramoto, M. Hashida, and S. Sakabe, "Single plasma mirror providing 10^4 contrast enhancement and 70% reflectivity for intense femtosecond lasers," Appl. Opt. **55**(21), 5647 (2016).
[29]M. Rehwald, S. Assenbaum, C. Bernert, F.-E. Brack, M. Bussmann, T. E. Cowan, C. B. Curry, F. Fiuza, M. Garten, L. Gaus, M. Gauthier, S. Göde, I. Göthel, S. H. Glenzer, L. Huang, A. Huebl, J. B. Kim, T. Kluge, S. Kraft, F. Kroll, J. Metzkes-Ng, T. Miethlinger, M. Loeser, L. Obst-Huebl, M. Reimold, H.-P. Schlenvoigt, C. Schoenwaelder, U. Schramm, M. Siebold, F. Treffert, L. Yang, T. Ziegler, and K. Zeil, "Ultra-short pulse laser acceleration of protons to 80 MeV from cryogenic hydrogen jets tailored to near-critical density," Nat. Commun. **14**, 4009 (2023).
[30]B. M. Hegelich, I. Pomerantz, L. Yin, H. C. Wu, D. Jung, B. J. Albright, D. C. Gautier, S. Letzring, S. Palaniyappan, R. Shah, K. Allinger, R. Hörlin, J. Schreiber, D. Habs, J. Blakeney, G. Dyer, L. Fuller, E. Gaul, E. McCary, A. R. Meadows, C. Wang, T. Ditmire, and J. C. Fernández, "Laser-driven ion acceleration from relativistically transparent nanotargets," New J. Phys. **15**, 085015 (2013).
[31]F. Wagner, O. Deppert, C. Brabetz, P. Fiala, A. Kleinschmidt, P. Poth, V. A. Schanz, A. Tebartz, B. Zielbauer, M. Roth, T. Stöhlker, and V. Bagnoud, "Maximum proton energy above 85 MeV from the relativistic interaction of laser pulses with micrometer thick CH_2 targets," Phys. Rev. Lett. **116**, 205002 (2016).
[32]N. P. Dover, T. Ziegler, S. Assenbaum, C. Bernert, S. Bock, F. E. Brack, T. E. Cowan, E. J. Ditter, M. Garten, L. Gaus, I. Goethel, G. S. Hicks, H. Kiriyama, T. Kluge, J. K. Koga, A. Kon, K. Kondo, S. Kraft, F. Kroll, H. F. Lowe, J. Metzkes-Ng, T. Miyatake, Z. Najmudin, T. Püschel, M. Rehwald, M. Reimold, H. Sakaki, H. P. Schlenvoigt, K. Shiokawa, M. E. P. Umlandt, U. Schramm, K. Zeil, and M. Nishiuchi, "Enhanced ion acceleration from transparency-driven foils demonstrated at two ultraintense laser facilities," Light. Sci. Appl. **12**, 71 (2023).
[33]Y. X. Geng, D. Wu, W. Yu, Z. M. Sheng, S. Fritzsche, Q. Liao, M. J. Wu, X. H. Xu, D. Y. Li, W. J. Ma, H. Y. Lu, Y. Y. Zhao, X. T. He, J. E. Chen, C. Lin, and X. Q. Yan, "Proton beams from intense laser-solid interaction: Effects of the target materials," Matter Radiat. Extremes **5**, 064402 (2020).
[34]S. Kar, H. Ahmed, R. Prasad, M. Cerchez, S. Brauckmann, B. Aurand, G. Cantono, P. Hadjisolomou, C. L. S. Lewis, A. Macchi, G. Nersisyan, A. P. L. Robinson, A. M. Schroer, M. Swantusch, M. Zepf, O. Willi, and M. Borghesi, "Guided post-acceleration of laser-driven ions by a miniature modular structure," Nat. Commun. **7**, 10792 (2016).
[35]F. Kroll, F.-E. Brack, C. Bernert, S. Bock, E. Bodenstein, K. Brüchner, T. E. Cowan, L. Gaus, R. Gebhardt, U. Helbig, L. Karsch, T. Kluge, S. Kraft, M. Krause, E. Lessmann, U. Masood, S. Meister, J. Metzkes-Ng, A. Nossula, J. Pawelke, J. Pietzsch, T. Püschel, M. Reimold, M. Rehwald, C. Richter, H.-P. Schlenvoigt, U. Schramm, M. E. P. Umlandt, T. Ziegler, K. Zeil, and E. Beyreuther, "Tumour irradiation in mice with a laser-accelerated proton beam," Nat. Phys. **18**, 316–322 (2022).
[36]P. Hilz, T. M. Ostermayr, A. Huebl, V. Bagnoud, B. Borm, M. Bussmann, M. Gallei, J. Gebhard, D. Haffa, J. Hartmann, T. Kluge, F. H. Lindner, P. Neumayr, C. G. Schaefer, U. Schramm, P. G. Thirolf, T. F. Rösch, F. Wagner, B. Zielbauer, and J. Schreiber, "Isolated proton bunch acceleration by a petawatt laser pulse," Nat. Commun. **9**, 423 (2018).
[37]A. Henig, S. Steinke, M. Schnürer, T. Sokollik, R. Hörlein, D. Kiefer, D. Jung, J. Schreiber, B. M. Hegelich, X. Q. Yan, J. Meyer-ter-Vehn, T. Tajima, P. V. Nickles, W. Sandner, and D. Habs, "Radiation-pressure acceleration of ion beams driven by circularly polarized laser pulses," Phys. Rev. Lett. **103**, 245003 (2009).
[38]J. Fuchs, P. Antici, E. d'Humieres, E. Lefebvre, M. Borghesi, E. Brambrink, C. A. Cecchetti, M. Kaluza, V. Malka, M. Manclossi, S. Meyroneinc, P. Mora, J. Schreiber, T. Toncian, H. Pepin, and P. Audebert, "Laser-driven proton scaling laws and new paths towards energy increase," Nat. Phys. **2**(1), 48–54 (2006).
[39]P. Mora, "Plasma expansion into a vacuum," Phys. Rev. Lett. **90**(18), 185002 (2003).
[40]M. Carrié, E. Lefebvre, A. Flacco, and V. Malka, "Influence of subpicosecond laser pulse duration on proton acceleration," Phys. Plasmas **16**(5), 053105 (2009).
[41]J. Fuchs, Y. Sentoku, E. d'Humières, T. E. Cowan, J. Cobble, P. Audebert, A. Kemp, A. Nikroo, P. Antici, E. Brambrink, A. Blazevic, E. M. Campbell, J. C. Fernández, J.-C. Gauthier, M. Geissel, M. Hegelich, S. Karsch, H. Popescu, N. Renard-LeGalloudec, M. Roth, J. Schreiber, R. Stephens, and H. Pepin, "Comparative spectra and efficiencies of ions laser-accelerated forward from the front and rear surfaces of thin solid foils," Phys. Plasmas **14**(5), 053105 (2007).
[42]A. A. Andreev, R. Sonobe, S. Kawata, S. Miyazaki, K. Sakai, K. Miyazuki, T. Kikuchi, K. Platonov, and K. Nemoto, "Effect of a laser prepulse on fast ion generation in the interaction of ultra-short intense laser pulses with a limited-mass foil target," Plasma Phys. Controlled Fusion **48**(11), 1605–1619 (2006).
[43]K. Zeil, S. D. Kraft, S. Bock, M. Bussmann, T. E. Cowan, T. Kluge, J. Metzkes, T. Richter, R. Sauerbrey, and U. Schramm, "The scaling of proton energies in ultrashort pulse laser plasma acceleration," New J. Phys. **12**(4), 045015 (2010).
[44]S. Fourmaux, S. Buffechoux, B. Albertazzi, D. Capelli, A. Lévy, S. Gnedyuk, L. Lecherbourg, P. Lassonde, S. Payeur, P. Antici, H. Pépin, R. S. Marjoribanks, J. Fuchs, and J. C. Kieffer, "Investigation of laser-driven proton acceleration using ultra-short, ultra-intense laser pulses," Phys. Plasmas **20**(1), 013110 (2013).